
Score Based Error Correcting Code Decoder

Alon Helvits¹ Eliya Nachmani¹

Abstract

Error-correcting codes enable reliable communication, yet practical soft decoding remains challenging across code families and block lengths. We propose SB-ECC, a score-based decoder that casts decoding as continuous-time denoising. A neural denoiser defines a probability-flow ordinary differential equation (ODE) that iteratively updates the noisy channel observation toward a valid codeword, guided by parity constraints. The model is trained across noise levels without time/SNR conditioning, enabling inference without SNR estimation and supporting a direct latency-accuracy trade-off controlled by the ODE solver budget. We use the raw signed channel observation as input for learning a continuous denoising field. Across 42 code/SNR settings, SB-ECC achieves the best BER in 39/42 entries, with an average SNR gain of 0.17 dB and a maximum gain of 0.46 dB over the strongest competing baseline, we showed that swapping the solver from Euler to DPM preserves $-\ln(\text{BER})$ while reducing end-to-end decoding time by 8.86% on average (up to 12.82%).

1. Introduction

Reliable digital communication relies on Error-Correcting Codes (ECC) that allow a receiver to reconstruct a transmitted codeword from a noisy channel observation. Although Maximum-Likelihood (ML) decoding is optimal, it is NP-hard for general linear block codes (Berlekamp et al., 2003), making practical soft decoding a central challenge for many code families and block lengths. Classical iterative decoders, most notably belief propagation (BP) (Richardson & Urbanke, 2002), perform approximate marginalization via message passing on a code’s factor/Tanner graph (Gallager,

1962; Kschischang et al., 2002).

Deep learning (LeCun et al., 2015) emerged as a compelling alternative for decoding, with two dominant lines of work. *Model-based* neural decoders start from an iterative algorithm (e.g., BP or min-sum) and “unroll” a fixed number of iterations into a trainable network, often learning iteration-dependent weights or offsets while preserving Tanner-graph structure (Nachmani et al., 2016; Cammerer et al., 2017; Lugosch & Gross, 2017; Nachmani et al., 2018; Lian et al., 2019; Buchberger et al., 2021). These methods benefit from strong inductive bias, but their computation and connectivity remain tied to the underlying iterative procedure, which can limit expressivity and scalability.

Model-free decoders instead learn the decoding function directly from data using different neural network architectures. Early model-free neural decoders therefore focused on short block lengths, learning a direct mapping from raw channel observations \mathbf{y} (or log-likelihood ratios (LLRs)) to the transmitted bits (Seo et al., 2018b; Leung et al., 2019b; Matsumine & Ochiai, 2024). A major difficulty is the combinatorial explosion of the output space. For a generic (n, k) code, the code-book size $|\mathcal{C}| = 2^k$ scales exponentially with the information length. Consequently, the available training data is inevitably sparse relative to the total volume of the codeword space, often leading to overfitting when training on raw channel observations (Bennatan et al., 2018). A key practical step that enabled modern model-free decoders is a symmetry-preserving pre-processing pipeline that utilizes reliability features, such as the magnitude $|\mathbf{y}|$ of the received signal \mathbf{y} together with parity information (e.g. hard-syndrome, soft-syndrome (Lau et al., 2025)), allowing training on a canonical transmitted codeword under BPSK symmetry (Bennatan et al., 2018). This paradigm enabled Transformer-based decoders that incorporate code structure through attention masking guided by the parity-check matrix. Error Correction Code Transformer (ECCT) introduced masked self-attention constrained by the parity-check graph to model long-range dependencies (Choukroun & Wolf, 2022b; Levy et al., 2024), and CrossMPT (Park et al., 2024) further improves scalability by treating magnitude and parity information as distinct modalities coupled via masked cross-attention blocks that emulate variable/check message exchange.

¹School of Electrical and Computer Engineering (ECE), Ben Gurion University, Beer Sheva, Israel. Correspondence to: Alon Helvits <alonhel@post.bgu.ac.il>, Eliya Nachmani <eliyanac@bgu.ac.il>.

In parallel, diffusion and score-based generative models have achieved remarkable success by learning to reverse a gradual noising process (Sohl-Dickstein et al., 2015; Song & Ermon, 2019; Ho et al., 2020; Song et al., 2020b). While these foundational works were developed primarily for continuous data such as images, diffusion models have since been successfully adapted to other modalities, including audio generation (Kong et al., 2020) and text generation (Li et al., 2022). Denoising Diffusion Error Correction Codes (DDECC) (Choukroun & Wolf, 2022a) adapted this viewpoint to channel decoding by interpreting transmission over noise as a forward diffusion process and decoding as an iterative denoising trajectory guided by code constraints, while still relying on magnitude-based reliability preprocessing.

In this work, we revisit the standard preprocessing choice from the perspective of score-based decoding. Mapping $\mathbf{y} \mapsto |\mathbf{y}|$ folds the observation space and removes directional information that may be beneficial when learning a continuous guidance field in \mathbb{R}^n . Conceptually, this also changes the learning problem, while many model-free decoders are trained to directly predict bit logits/LLRs (Choukroun & Wolf, 2022a;b; Park et al., 2024), we train a continuous denoising model that regresses an additive-noise (equivalently, score) vector field in \mathbb{R}^n (Song et al., 2020b). We therefore propose a score-based decoding framework, **SB-ECC** (*Score-Based Error-Correcting Code Decoder*), that trains and operates directly on the *signed* received signal \mathbf{y} . We formulate decoding under a variance-exploding (VE) construction in continuous time (Song et al., 2020b), and train a neural score model to predict additive noise (equivalently, the score under the VE marginal) conditioned on the noisy observation and code constraints.

A practical challenge in this setting is that the effective noise level (and thus the corresponding diffusion “time”) is not known at inference time, since the channel SNR is typically unavailable. Rather than estimating time explicitly, we use a *time-unconditional* score model trained across a range of noise levels, together with a simple *linear noise schedule*. This removes any need for SNR side information and avoids committing to a specific test-time noise calibration. Our approach naturally supports flexible inference, the number of solver steps (or function evaluations) can be chosen to trade accuracy for latency without changing the trained model, and without requiring a time/SNR input.

Our main contributions are:

1. We introduce SB-ECC, a time-unconditional score-based decoder for linear block codes that learns a continuous additive-noise (score) field directly on the signed channel observation and performs decoding via Probability-Flow ODE (PF-ODE) integration guided by parity constraints.

2. We speed up PF-ODE decoding by replacing the Euler solver with DPM-Solver while preserving performance. This is enabled by our linear noise schedule and uniform σ -space discretization, which are naturally suited to time-unconditional decoding.
3. Across multiple code families and SNRs, we improve over strong neural baselines, achieving the best BER in 39/42 entries with an average SNR gain of 0.17 dB and a maximum gain of 0.46 dB over the strongest competing baseline.

Reproducibility. Code for training and evaluation is available at <https://github.com/alonhelvits/SB-ECC>.

2. Related Works

Neural decoders for error-correcting codes are often divided into *model-based* (model-driven) and *model-free* approaches. Model-based methods start from iterative decoders such as belief propagation (BP) or min-sum (MS) and unroll a fixed number of message-passing iterations into a trainable network while preserving the Tanner-graph computation (Nachmani et al., 2016; Cammerer et al., 2017; Lugosch & Gross, 2017; Nachmani et al., 2018; Lian et al., 2019; Buchberger et al., 2021). For BP, (Nachmani et al., 2016) learns edge- and/or iteration-dependent parameters within an unrolled Tanner-graph decoder. For MS, offset min-sum variants retain the same message-passing structure but learn additive *offset* corrections (Lugosch & Gross, 2017). More expressive hybrids modify the update rules beyond simple scalings/offsets, e.g., via hypernetwork-style parameterizations, autoregressive messaging, or learned decimation mechanisms (Nachmani & Wolf, 2019; 2021; Buchberger et al., 2021).

Unlike model-based decoders, *model-free* neural decoders learn the mapping from the noisy channel observation directly using flexible architectures, without committing to a particular iterative algorithm. This line of work dates back to early neural decoding efforts (e.g., NN realizations/approximations of classical decoders and recurrent decoders for convolutional codes) (Wang & Wicker, 1996; Hamalainen & Henriksson, 1999). Modern deep-learning-era model-free decoders typically use fully connected or recurrent architectures that ingest the received soft vector \mathbf{y} (O’Shea & Hoydis, 2017; Gruber et al., 2017; Seo et al., 2018a). While these approaches can perform well on short block lengths, they often face sample-complexity and generalization challenges as n grows, and their performance can be sensitive to architecture choice (MLP vs CNN vs RNN/LSTM) and latency constraints (Lyu et al., 2018; Satiraju et al., 2018; Leung et al., 2019a).

The introduction of magnitude (reliability) and syndrome

preprocessing often framed as learning a *multiplicative* noise model was crucial for mitigating overfitting and enabling model-free decoders to scale beyond very short codes (Benatan et al., 2018; Kamassury & Silva, 2020; Artemasov et al., 2023). Complementary directions for improving robustness and generalization include fast adaptation via meta-learning and transfer learning (Jiang et al., 2019; Lee et al., 2020). Building on this paradigm, Choukroun & Wolf (2022b) introduced the Error Correction Code Transformer (ECCT), where masked self-attention injects parity-check structure into a Transformer decoder, marking a major step in demonstrating that model-free neural decoders can outperform classical and model-based baselines. Subsequent work strengthened the masking/conditioning mechanism with systematic and double-masking strategies (Park et al., 2023), explored joint encoder–decoder (end-to-end code + decoder) optimization (Choukroun & Wolf, 2024b), proposed a foundation model aimed at stronger zero-shot generalization across codes and lengths (Choukroun & Wolf, 2024a), and introduced cross-attention/message-passing variants that improve performance and efficiency on longer codes (Park et al., 2024; Cohen et al., 2025). In parallel, generative diffusion-based decoders such as Denoising Diffusion Error Correction Codes (DDECC) formulate decoding as iterative denoising with code constraints, offering a complementary paradigm with strong results across multiple code families (Choukroun & Wolf, 2022a). More recently, Lei et al. (2025) proposed an error-correction consistency-flow model that distills the denoising trajectory into one-step decoding, emphasizing low-latency inference as an alternative to iterative diffusion-based decoding.

Diffusion and score-based generative models evolved from early formulations that learn a reverse-time denoising process for a progressive noising (diffusion) forward process (Sohl-Dickstein et al., 2015), to practical large-scale diffusion models such as DDPM (Ho et al., 2020) and a series of improved training/sampling variants (Song et al., 2020a; Nichol & Dhariwal, 2021; Dhariwal & Nichol, 2021; Rombach et al., 2022; Saharia et al., 2022). In parallel, score-based generative modeling framed generation as estimating $\nabla_{\mathbf{x}} \log p_t(\mathbf{x})$ across noise levels (Hyvärinen, 2005; Vincent, 2011; Song & Ermon, 2019), and later unified in continuous time through the Score-SDE framework, where samples are obtained by numerically solving a reverse-time Stochastic Differential Equation (SDE) or its probability-flow Ordinary Differential Equation (ODE) (Song et al., 2020b). A major practical driver has been sampler/solver design, where the number of function evaluations trades off quality and latency. Examples include standard discretizations used in score-based sampling (e.g., Euler–Maruyama / predictor–corrector) (Song et al., 2020b) and EDM-style design choices such as Heun-based samplers and reparameterizations/preconditioning (Karras et al., 2022), and dedicated

high-order ODE solvers such as PNDM and DPM-Solver (Liu et al., 2022; Lu et al., 2022), as well as subsequent refinements (e.g., DPM-Solver++) (Zheng et al., 2023). While these methods were first developed and popularized primarily for high-fidelity image generation (Ho et al., 2020; Song et al., 2020a; Nichol & Dhariwal, 2021; Dhariwal & Nichol, 2021; Rombach et al., 2022; Saharia et al., 2022), diffusion/score-based modeling has since been successfully adapted to other modalities, including audio and speech synthesis (Chen et al., 2020; Kong et al., 2020; Popov et al., 2021), language and other discrete data (Austin et al., 2021; Li et al., 2022), and video generation (Ho et al., 2022a;b; Blattmann et al., 2023a;b).

3. Preliminaries and Background

Here we provide necessary background on error correction coding, diffusion and score-based models.

3.1. Error Correction Codes

We consider a standard coded transmission using a binary linear block code C . The code is specified by a generator matrix $G \in \{0, 1\}^{k \times n}$ and a parity-check matrix $H \in \{0, 1\}^{(n-k) \times n}$ such that $GH^T = 0$ over $\text{GF}(2)$ (equivalently, $H\mathbf{x}^T = \mathbf{0}$ for all $\mathbf{x} \in C$) (Richardson & Urbanke, 2008). Given a message $\mathbf{m} \in \{0, 1\}^k$, the encoder produces a codeword $\mathbf{x} = \mathbf{m}G \in C \subseteq \{0, 1\}^n$ satisfying $H\mathbf{x}^T = \mathbf{0}$.

We focus on Binary Phase Shift Keying (BPSK) modulation over Additive White Gaussian Noise (AWGN), as commonly adopted in deep decoders (Choukroun & Wolf, 2022b). Let $\mathbf{x}_s \in \{\pm 1\}^n$ denote the BPSK-modulated codeword (e.g., $\mathbf{x}_s = \mathbf{1} - 2\mathbf{x}$). The receiver observes

$$\mathbf{y} = \mathbf{x}_s + \mathbf{z}, \quad (1)$$

where $\mathbf{z} \sim \mathcal{N}(\mathbf{0}, \sigma_{\text{ch}}^2 I_n)$ and $\sigma_{\text{ch}} > 0$ is the channel noise standard deviation determined by the channel condition, yielding a soft observation $\mathbf{y} \in \mathbb{R}^n$.

A convenient baseline is the hard-decision estimate obtained by element-wise thresholding: $\hat{\mathbf{x}}_s = \text{sign}(\mathbf{y}) \in \{\pm 1\}^n$, mapped back to bits $\mathbf{y}_b = \text{bin}(\hat{\mathbf{x}}_s) \in \{0, 1\}^n$. Here, $\text{sign}(y_i) = +1$ if $y_i \geq 0$ and -1 otherwise, and $\text{bin}(+1) = 0$ and $\text{bin}(-1) = 1$ (applied element-wise). Parity consistency of this hard decision is tested via the syndrome $\mathbf{s}(\mathbf{y}) \triangleq H\mathbf{y}_b^T \in \{0, 1\}^{n-k}$ over $\text{GF}(2)$. If $\mathbf{s}(\mathbf{y}) = \mathbf{0}$ then $\mathbf{y}_b \in C$ is a valid codeword; otherwise, $\mathbf{s}(\mathbf{y}) \neq \mathbf{0}$ indicates violated constraints. When the parity checks fail, a decoder $f: \mathbb{R}^n \rightarrow \{0, 1\}^n$ uses the soft observation \mathbf{y} to produce a refined estimate of the transmitted codeword $\hat{\mathbf{x}} = f(\mathbf{y})$. The decoder output is validated by the same parity checks via its syndrome $H\hat{\mathbf{x}}^T$, and successful decoding corresponds to $H\hat{\mathbf{x}}^T = \mathbf{0}$.

Algorithm 1 Training procedure for Score-Based Error Correction Codes

Require: Batch \mathbf{x}_0 , schedule $\sigma(\cdot)$, learning rate η

- 1: Initialize parameters θ
- 2: **repeat**
- 3: Sample $t \sim \mathcal{U}(0, 1)$ and $\epsilon \sim \mathcal{N}(\mathbf{0}, \mathbf{I})$
- 4: $\sigma \leftarrow \sigma(t)$, $\mathbf{y} \leftarrow \mathbf{x}_0 + \sigma \epsilon$
- 5: $\mathbf{s} \leftarrow \mathbf{H} \text{bin}(\text{sign}(\mathbf{y}))^\top \bmod 2$
- 6: $\mathcal{L}_\epsilon \leftarrow \|\hat{\epsilon}_\theta(\mathbf{y}, \mathbf{s}) - \epsilon\|_2^2$
- 7: $\theta \leftarrow \theta - \eta \nabla_\theta \mathcal{L}_\epsilon$
- 8: **until** convergence

3.2. Diffusion and Score-Based Generative Models

Diffusion Models (Discrete-Time View). Diffusion models specify a *forward* noising process that forms a Markov chain $q(\mathbf{x}_{1:T} | \mathbf{x}_0) = \prod_{t=1}^T q(\mathbf{x}_t | \mathbf{x}_{t-1})$, where each transition gradually corrupts the signal by adding Gaussian noise (Ho et al., 2020). Because these Gaussian transitions compose in closed form, one can equivalently write the marginal perturbation at (continuous) time t as

$$\mathbf{x}_t = \alpha(t) \mathbf{x}_0 + \sigma(t) \epsilon, \quad \epsilon \sim \mathcal{N}(\mathbf{0}, I_n), \quad (2)$$

where $\alpha(t)$ and $\sigma(t)$ define the noise schedule. Many diffusion models are trained to predict the injected noise ϵ (or equivalently \mathbf{x}_0), which is closely related to the score under Gaussian perturbations (Song et al., 2020b; Ho et al., 2020; Karras et al., 2022). In this work we use the continuous-time score-based formulation below, which expresses the same Gaussian perturbation family via a stochastic differential equation (SDE) and enables sampling through its associated probability-flow ODE (Song et al., 2020b).

Forward Diffusion as an SDE. Score-based generative models define a continuous noising process over $t \in [0, T]$ via an Itô SDE (Song et al., 2020b):

$$d\mathbf{x}_t = f(\mathbf{x}_t, t) dt + g(t) d\mathbf{w}_t, \quad (3)$$

where $\mathbf{x}_t \in \mathbb{R}^n$ is the state at time t , $f(\mathbf{x}_t, t)$ is the drift field, $g(t)$ is the diffusion amplitude, and \mathbf{w}_t is a standard n -dimensional Wiener process. The terminal time T controls the overall noise level. A common choice is the variance-exploding (VE) SDE (Song et al., 2020b), where $f(\mathbf{x}, t) = \mathbf{0}$ and the noise scale $\sigma(t)$ increases with t . Choosing $g(t)$ such that $g(t)^2 = \frac{d\sigma(t)^2}{dt}$ yields the marginal perturbation form

$$\mathbf{x}_t = \mathbf{x}_0 + \sigma(t)\epsilon, \quad \epsilon \sim \mathcal{N}(\mathbf{0}, I_n). \quad (4)$$

This is particularly natural for channel decoding, the AWGN channel in (1) corresponds to a VE perturbation at a specific noise level, i.e., there exists t^* such that $\sigma(t^*) = \sigma_{\text{ch}}$.

Algorithm 2 Decoding with early exit

Require: Received vector $\mathbf{y} \in \mathbb{R}^n$, parity-check matrix $\mathbf{H} \in \{0, 1\}^{(n-k) \times n}$, steps N_{steps} , endpoints $\sigma_{\text{max}} \rightarrow \sigma_{\text{min}}$

- 1: $\Delta\sigma \leftarrow (\sigma_{\text{max}} - \sigma_{\text{min}})/N_{\text{steps}}$
- 2: $\mathbf{x}^{(0)} \leftarrow \mathbf{y}$
- 3: **for** $i = 0, \dots, N_{\text{steps}} - 1$ **do**
- 4: $\hat{\mathbf{c}}_s \leftarrow \text{sign}(\mathbf{x}^{(i)}) \{\hat{\mathbf{c}}_s \in \{\pm 1\}^n\}$
- 5: $\hat{\mathbf{c}} \leftarrow \text{bin}(\hat{\mathbf{c}}_s) \{\hat{\mathbf{c}} \in \{0, 1\}^n\}$
- 6: $\mathbf{s} \leftarrow \mathbf{H}\hat{\mathbf{c}}^\top \bmod 2 \{\mathbf{s} \in \{0, 1\}^{n-k}\}$
- 7: **if** $\mathbf{s} = \mathbf{0}$ **then**
- 8: **break**
- 9: **end if**
- 10: $\hat{\mathbf{c}} \leftarrow \hat{\epsilon}_\theta(\mathbf{x}^{(i)}, \mathbf{s})$
- 11: $\mathbf{x}^{(i+1)} \leftarrow \mathbf{x}^{(i)} - \Delta\sigma \hat{\mathbf{c}}$
- 12: **end for**
- 13: **return** $\text{bin}(\text{sign}(\mathbf{x}^{(i)}))$

Score Function and Reverse-Time Dynamics. Let $\{\mathbf{x}_t\}_{t \in [0, T]}$ follow the forward SDE in (3), and let $p_t(\mathbf{x})$ be the resulting marginal density at time t . The *score* is the gradient of the log-density $\nabla_{\mathbf{x}} \log p_t(\mathbf{x})$. Score-based models learn a neural approximation $s_\theta(\mathbf{x}, t) \approx \nabla_{\mathbf{x}} \log p_t(\mathbf{x})$ from noisy samples at different noise levels. Given access to the score, one can construct a reverse-time stochastic process whose marginals evolve from a simple noise distribution at $t = T$ back to the data distribution at $t = 0$ (Song et al., 2020b):

$$d\mathbf{x}_t = \left[f(\mathbf{x}_t, t) - g(t)^2 \nabla_{\mathbf{x}} \log p_t(\mathbf{x}_t) \right] dt + g(t) d\bar{\mathbf{w}}_t, \quad (5)$$

where $d\bar{\mathbf{w}}_t$ is a reverse-time Wiener increment. Instead of sampling the reverse SDE, one may integrate the probability flow ODE (PF-ODE), a deterministic dynamics that shares the same marginals $\{p_t\}$ as the SDE (Song et al., 2020b):

$$d\mathbf{x}_t = \left[f(\mathbf{x}_t, t) - \frac{1}{2}g(t)^2 \nabla_{\mathbf{x}} \log p_t(\mathbf{x}_t) \right] dt. \quad (6)$$

In practice, we replace the intractable score by a learned network $s_\theta(\mathbf{x}, t)$ and integrate the resulting reverse dynamics. In our setting we use the VE construction, where $f(\mathbf{x}, t) = \mathbf{0}$ and $g(t)^2 = \frac{d\sigma(t)^2}{dt}$, and we implement decoding by integrating the PF-ODE.

Denoising Score Matching (DSM) Objective. Score-based models are commonly trained via (denoising) score matching (Hyvärinen, 2005; Song et al., 2020b). Under the VE marginal (4) the conditional score admits a closed form (Song et al., 2020b):

$$\nabla_{\mathbf{x}_t} \log p(\mathbf{x}_t | \mathbf{x}_0) = -\frac{\mathbf{x}_t - \mathbf{x}_0}{\sigma(t)^2} = -\frac{\epsilon}{\sigma(t)}. \quad (7)$$

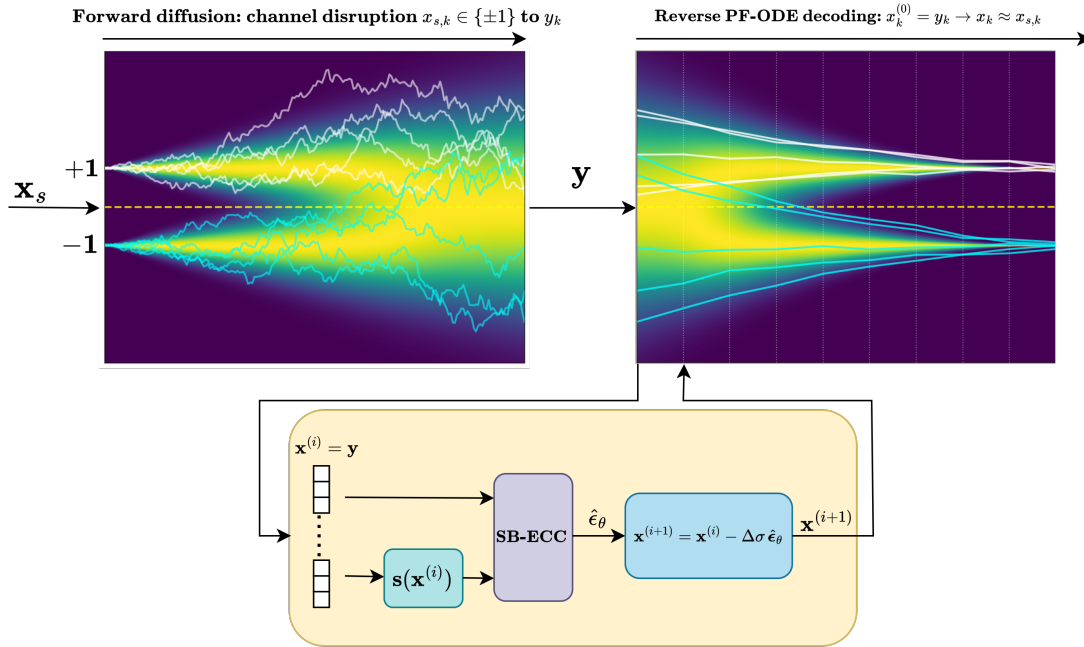


Figure 1. Per-bit view of decoding as deterministic denoising. **Left:** forward corruption (channel as a forward diffusion): each curve is one coordinate k , where a clean BPSK symbol $x_{s,k} \in \{\pm 1\}$ is perturbed into $y_k = x_{s,k} + z_k$ as the noise level increases. **Right:** reverse probability-flow ODE (PF-ODE) decoding: starting from $x_k^{(0)} = y_k$, the learned denoiser (with parity/syndrome guidance) drives each coordinate toward a valid codeword, concentrating mass back near ± 1 . Background heatmaps depict empirical marginal density over coordinates, and the dashed line marks the hard-decision boundary at 0.

A standard DSM objective is

$$\mathcal{L}_{\text{DSM}}(\theta) = \mathbb{E}_{t, \mathbf{x}_0, \varepsilon} \left[\lambda(t) \left\| s_\theta(\mathbf{x}_t, t) - \nabla_{\mathbf{x}_t} \log p(\mathbf{x}_t | \mathbf{x}_0) \right\|_2^2 \right], \quad (8)$$

which, using (7), is equivalent to

$$\mathcal{L}_{\text{DSM}}(\theta) = \mathbb{E}_{t, \mathbf{x}_0, \varepsilon} \left[\lambda(t) \left\| s_\theta(\mathbf{x}_t, t) + \frac{\varepsilon}{\sigma(t)} \right\|_2^2 \right]. \quad (9)$$

In practice, many works (Ho et al., 2020; Dhariwal & Nichol, 2021; Karras et al., 2022) adopt equivalent parameterizations, e.g., predicting the noise ε (or \mathbf{x}_0) instead of the score, since under the VE marginal these are related by $s_\theta(\mathbf{x}_t, t) \approx -\hat{\varepsilon}_\theta(\mathbf{x}_t, t)/\sigma(t)$ up to a time-dependent scaling (Song et al., 2020b).

4. Method

We propose a score-based decoding framework for binary linear block codes that operates directly on the full signed channel observation. Under BPSK over AWGN, the transmitted bit-codeword $\mathbf{x} \in \{0, 1\}^n$ is mapped to $\mathbf{x}_s \in \{\pm 1\}^n$ (e.g., $\mathbf{x}_s = \mathbf{1} - 2\mathbf{x}$), and the receiver observes

$$\mathbf{y} = \mathbf{x}_s + \mathbf{z}, \quad \mathbf{z} \sim \mathcal{N}(\mathbf{0}, \sigma_{\text{ch}}^2 I_n). \quad (10)$$

Many model-free decoders first preprocess \mathbf{y} into a *reliability-only* representation using $|\mathbf{y}|$ together with parity

information derived from hard decisions (e.g., a syndrome) (Bennatan et al., 2018; Choukroun & Wolf, 2022b; Park et al., 2024). This pre-processing improves generalization in deep decoders by providing symmetry-consistent reliability features while injecting code constraints through hard-decision parity information (Bennatan et al., 2018). In a score-based formulation, however, the model is used as a *continuous* denoising/score field in \mathbb{R}^n (to be integrated by an SDE/ODE solver), and the mapping $\mathbf{y} \mapsto |\mathbf{y}|$ is non-invertible: it collapses each equivalence class $\{\mathbf{s} \odot \mathbf{y} : \mathbf{s} \in \{\pm 1\}^n\}$ (size 2^n) to the same input, i.e., $|\mathbf{s} \odot \mathbf{y}| = |\mathbf{y}|$ for all \mathbf{s} , discarding per-coordinate directional information. An overview of our formulation is shown in Figure 1, we interpret the channel observation as a forward VE perturbation (left) and decode by integrating the reverse PF-ODE in σ -space using the learned denoiser with parity guidance (right). In principle, parity cues such as a hard-decision syndrome can partially disambiguate these equivalence classes, and we do not claim that learning the score from $(|\mathbf{y}|, \mathbf{s}(\mathbf{y}))$ is impossible. Rather, we treat signed observations as a modeling choice that preserves geometry and quantify its impact empirically (Section 5.3).

Transmission as forward diffusion. Following the diffusion view of decoding (Choukroun & Wolf, 2022a), we align the AWGN observation with a VE perturbation pro-

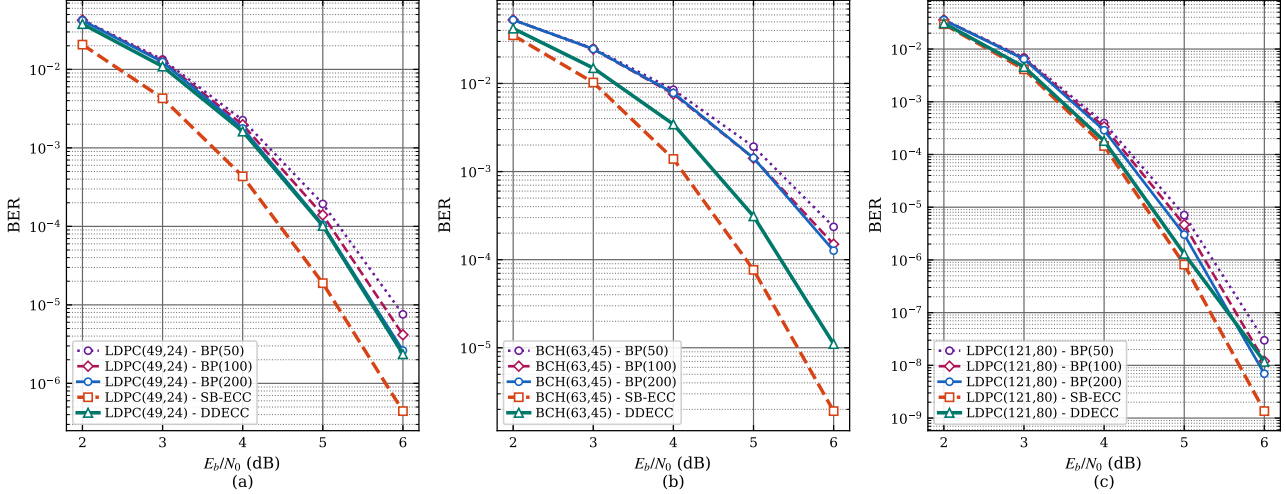


Figure 2. BER versus E_b/N_0 for representative code instances: (a) LDPC(49, 24), (b) BCH(63, 45), and (c) LDPC(121, 80). The curves compare SB-ECC, DDECC, and BP decoding with 50, 100, and 200 iterations.

cess. Let $\mathbf{x}_0 \in \{\pm 1\}^n$ denote a clean BPSK codeword and define a noisy state $\mathbf{x}_t = \mathbf{x}_0 + \sigma(t)\epsilon$, $\epsilon \sim \mathcal{N}(\mathbf{0}, I_n)$, such that the channel observation corresponds to $\mathbf{y} \equiv \mathbf{x}_t$ at some (unknown) noise level $\sigma(t^*) = \sigma_{\text{ch}}$.

Noise schedule. We parameterize the VE noise level by $t \in [0, 1]$ using a simple linear schedule (Karras et al., 2022):

$$\sigma(t) = \sigma_{\min} + (\sigma_{\max} - \sigma_{\min})t. \quad (11)$$

Here, σ_{\min} and σ_{\max} are fixed hyperparameters that set the minimum and maximum noise levels used during training and sampling. This induces the Gaussian forward kernel $p(\mathbf{x}_t | \mathbf{x}_0) = \mathcal{N}(\mathbf{x}_t; \mathbf{x}_0, \sigma^2(t)I)$.

4.1. Model

We use the CrossMPT architecture (Park et al., 2024), which represents decoding as interactions between *variable-node* (VN) tokens and *check-node* (CN) tokens coupled through the Tanner graph. CrossMPT treats VN features and CN features (syndrome/parity information) as separate modalities and uses masked attention to restrict message exchange to edges indicated by the parity check matrix H . All CN features and Tanner-graph masking are identical to CrossMPT; only the VN observation channel is changed from magnitude-only to signed. Unlike reliability-based decoders that output bit logits or bit-flip probabilities, our network outputs a *continuous* denoising direction $\hat{\epsilon}_\theta(\mathbf{y}, \mathbf{s}(\mathbf{y})) \in \mathbb{R}^n$

4.2. Training Objective

We train with the standard diffusion noise-parameterization (Ho et al., 2020). During training we sample a clean

BPSK codeword $\mathbf{x}_0 \in \{\pm 1\}^n$, draw $t \sim \mathcal{U}(0, 1)$ and $\epsilon \sim \mathcal{N}(\mathbf{0}, I_n)$, and construct $\mathbf{y} = \mathbf{x}_0 + \sigma(t)\epsilon$. We compute the corresponding syndrome $\mathbf{s}(\mathbf{y})$ and minimize the noise prediction loss

$$\mathcal{L}_\epsilon = \mathbb{E} \left[\|\hat{\epsilon}_\theta(\mathbf{y}, \mathbf{s}(\mathbf{y})) - \epsilon\|_2^2 \right]. \quad (12)$$

This objective is equivalent (up to a known noise-level scaling) to denoising score matching for Gaussian perturbations (Song & Ermon, 2019; Song et al., 2020b), and yields a denoiser/score surrogate that can be used inside our iterative decoding dynamics (described next in Section 4.3).

4.3. Inference

Our inference process reverses the diffusion process to recover the clean BPSK codeword $\mathbf{x}_0 \in \{\pm 1\}^n$ from the received vector \mathbf{y} . We integrate the PF-ODE in *symbol space* (BPSK), and obtain decoded bits by $\hat{\mathbf{x}} = \text{bin}(\text{sign}(\mathbf{x}^{(N_{\text{steps}})}))$ (or the early-stopped iterate). Following the VE formulation, this can be viewed as solving the probability flow ODE (PF-ODE) associated with the VE-SDE (Song et al., 2020b).

$$d\mathbf{x} = -\frac{1}{2} \frac{d[\sigma^2(t)]}{dt} \nabla_{\mathbf{x}} \log p_t(\mathbf{x}) dt. \quad (13)$$

Using $d\sigma^2(t)/dt = 2\sigma(t)\dot{\sigma}(t)$ and the VE relation $\nabla_{\mathbf{x}} \log p_t(\mathbf{x}) \approx -\hat{\epsilon}_\theta(\mathbf{x}, \mathbf{s}(\mathbf{x}))/\sigma(t)$ under Gaussian perturbations, we obtain an equivalent PF-ODE written in σ -space $d\mathbf{x} = \hat{\epsilon}_\theta(\mathbf{x}, \mathbf{s}(\mathbf{x})) d\sigma$. We integrate from σ_{\max} down to σ_{\min} (hence $d\sigma < 0$), yielding a deterministic trajectory that progressively removes noise.

Scheduling without time conditioning. Standard diffusion samplers often discretize the *time* interval $t \in [0, 1]$

Score Based Error Correcting Code Decoder

Table 1. Main decoding results across BCH, Polar, LDPC, MacKay, and CCSDS codes for BP, AR-BP (Nachmani & Wolf, 2021), CrossMPT (Park et al., 2024), DDECC (Choukroun & Wolf, 2022a), and SB-ECC. Results are reported as $-\ln(\text{BER})$ at $E_b/N_0 \in \{4, 5, 6\}$ dB, where higher is better. DDECC and SB-ECC use the same CrossMPT backbone for a controlled method-level comparison. BP and AR-BP results use 50 decoding iterations, except for gray AR-BP entries, which use 5 iterations. The best result is marked in **bold** and the second-best result is underlined.

Architecture		BP-based decoders						Model-free decoders								
Code Type	Params	BP			AR BP			CrossMPT			DDECC			SB-ECC (Ours)		
		4	5	6	4	5	6	4	5	6	4	5	6	4	5	6
BCH	(63,36)	4.03	5.42	7.26	4.57	6.39	8.92	5.03	6.91	9.37	<u>5.30</u>	<u>7.32</u>	<u>10.25</u>	5.74	8.12	11.20
	(63,45)	4.36	5.55	7.26	4.97	6.90	9.41	<u>5.90</u>	<u>8.20</u>	<u>11.62</u>	5.67	8.07	11.41	6.58	9.48	13.17
	(63,51)	4.50	5.82	7.42	5.17	7.16	9.53	<u>5.78</u>	<u>8.08</u>	<u>11.41</u>	5.37	7.48	10.51	6.19	8.82	12.45
POLAR	(64,32)	4.26	5.38	6.50	5.57	7.43	9.82	<u>7.50</u>	<u>9.97</u>	<u>13.31</u>	7.03	9.69	12.97	7.77	10.30	13.78
	(64,48)	4.74	5.94	7.42	5.41	7.19	9.30	<u>6.51</u>	8.70	11.31	6.07	8.40	10.90	6.63	8.64	<u>11.27</u>
	(128,64)	4.10	5.11	6.15	4.84	6.78	9.30	7.52	11.21	14.76	<u>8.16</u>	<u>12.04</u>	<u>16.27</u>	9.03	13.13	16.94
	(128,86)	4.49	5.65	6.97	5.39	7.37	10.13	7.51	10.83	15.24	<u>7.92</u>	<u>11.34</u>	<u>15.61</u>	8.03	11.48	16.10
	(128,96)	4.61	5.79	7.08	5.27	7.44	10.20	7.15	<u>10.15</u>	13.13	<u>7.24</u>	10.32	<u>13.26</u>	7.64	10.32	13.37
LDPC	(49,24)	6.23	8.19	11.72	6.58	9.39	12.39	<u>6.68</u>	<u>9.52</u>	<u>13.19</u>	6.26	9.07	12.71	7.74	10.88	14.63
	(121,60)	5.64	8.88	13.33	5.22	8.31	13.07	5.74	9.26	14.78	<u>6.22</u>	<u>10.18</u>	<u>15.89</u>	6.33	10.38	16.38
	(121,70)	6.91	10.66	15.62	6.45	10.01	14.77	7.06	11.39	17.52	<u>7.64</u>	<u>12.30</u>	<u>17.98</u>	7.75	12.69	19.24
	(121,80)	7.84	11.86	17.33	7.22	11.03	15.90	7.99	12.75	18.15	<u>8.62</u>	<u>13.55</u>	<u>18.26</u>	8.84	14.02	20.42
MacKay	(96,48)	6.84	9.40	12.57	7.43	10.65	14.65	7.97	11.77	15.52	<u>8.58</u>	<u>12.48</u>	<u>16.04</u>	8.97	12.82	16.25
CCSDS	(128,64)	8.00	12.11	17.17	7.25	10.99	16.36	7.68	11.88	<u>17.50</u>	<u>8.40</u>	<u>13.18</u>	17.47	8.60	13.43	19.20

using a fixed grid, which typically induces *non-uniform* increments in the corresponding noise level $\sigma(t)$. This is natural for time-conditional models that start from a known t (usually $t = T = 1$). In channel decoding, however, the received vector $\mathbf{y} = \mathbf{x}_0 + \sigma^* \mathbf{z}$ lies at an *unknown* intermediate noise level σ^* , and our denoiser is not conditioned on t (nor on σ^*). To avoid locating \mathbf{y} on a non-uniform t -grid, we discretize *directly* in σ .

Uniform discretization in σ -space. With the linear schedule in Eq. (11), a uniform grid $t_k = \frac{k}{N_{\text{steps}}}$ induces

$$\begin{aligned} \sigma_k &= \sigma_{\min} + (\sigma_{\max} - \sigma_{\min}) \frac{k}{N_{\text{steps}}}, \\ \Delta\sigma &= \frac{\sigma_{\max} - \sigma_{\min}}{N_{\text{steps}}}. \end{aligned} \quad (14)$$

The hyperparameter N_{steps} therefore controls the runtime–accuracy trade-off.

Discrete solver and early stopping. Starting from $\mathbf{x}^{(0)} = \mathbf{y}$, we apply Euler updates in σ -space:

$$\mathbf{x}^{(i+1)} = \mathbf{x}^{(i)} - \Delta\sigma \hat{\epsilon}_\theta(\mathbf{x}^{(i)}, \mathbf{s}(\mathbf{x}^{(i)})) \quad (15)$$

We apply (15) $i = 0, \dots, N_{\text{steps}} - 1$, after each step we form a hard decision and compute the syndrome; if $\mathbf{s}(\mathbf{x}^{(i)}) = \mathbf{0}$,

we terminate early and output the corresponding codeword. Otherwise, we continue up to the maximum budget N_{steps} . We also evaluate higher-order solvers, such as DPM-Solver (Lu et al., 2022), under the same $\Delta\sigma$ discretization to study performance–latency trade-offs in Section 5.2.

5. Experiments

We evaluate our score-based decoder on standard linear block code benchmarks and compare against strong neural and classical baselines. We also study inference-time trade-offs by varying the ODE solver and step budget.

5.1. Experimental Setup

Codes and model configuration. We follow common neural-decoding benchmarks and report results on Polar codes (Arikan, 2009), LDPC codes (Gallager, 1962), BCH codes (Bose & Ray-Chaudhuri, 1960), MacKay codes, and CCSDS codes. Unless stated otherwise, all model-free entries use the same backbone scale ($N = 6$ attention layers, $d = 128$ hidden dimension), matching the main CrossMPT configuration. For a fair method-level comparison with diffusion-based decoding, we retrain DDECC (Choukroun & Wolf, 2022a) using the same CrossMPT backbone as

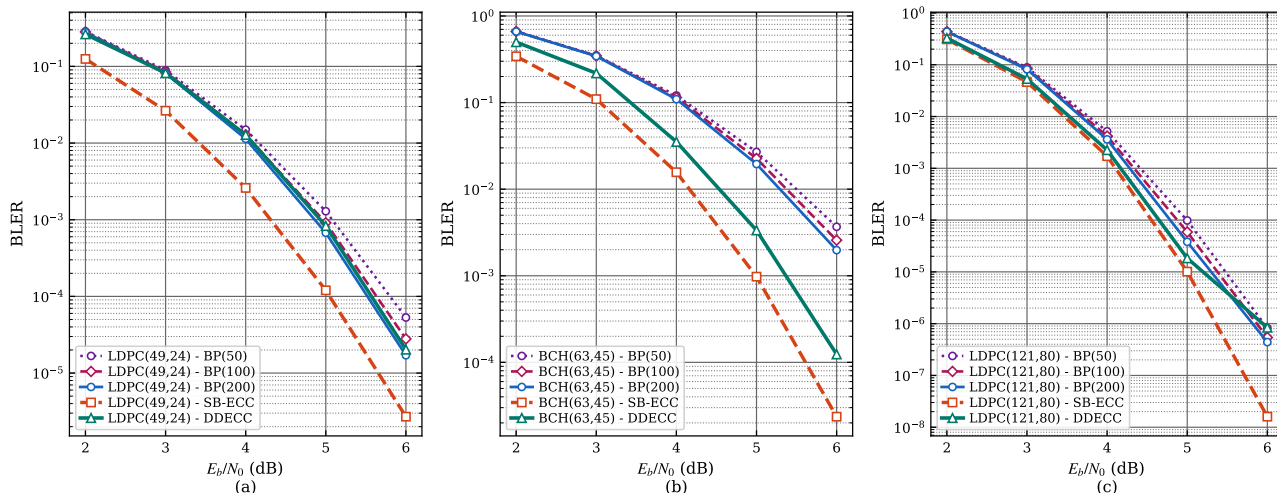


Figure 3. BLER versus E_b/N_0 for representative code instances: (a) LDPC(49, 24), (b) BCH(63, 45), and (c) LDPC(121, 80). The curves compare SB-ECC, DDECC, and BP decoding with 50, 100, and 200 iterations.

SB-ECC.

Training details. All models are trained with Adam (Kingma & Ba, 2014) optimizer, learning rate 5×10^{-4} and cosine annealing. We use batch size of 256 for codes with $n \leq 64$ and 128 for longer codes. We train for 1500 epochs with 1000 batches per epoch. Training samples are generated on-the-fly via BPSK over AWGN using a linear noise schedule $\sigma(t)$ with $\sigma_{\min} = 0.1$ and $\sigma_{\max} = 0.8$. Unless stated otherwise, inference uses Euler with $N_{\text{steps}} = 10$.

Evaluation protocol and metric. We report $-\ln(\text{BER})$ (higher is better) at $E_b/N_0 \in \{4, 5, 6\}$ dB. For each SNR, we decode until observing 500 frame errors or processing 10^8 frames (10^9 for LDPC). When summarizing overall improvements, we also report SNR gain (dB), defined as the horizontal E_b/N_0 shift required for the strongest prior method to match our BER, computed by interpolation between the evaluated E_b/N_0 points.

Baselines. We compare against BP, AR-BP (Nachmani & Wolf, 2021), CrossMPT (Park et al., 2024), and DDECC (Choukroun & Wolf, 2022a). BP and AR-BP results are reported using 50 decoding iterations, except for the gray AR-BP entries, which correspond to the 5-iteration results reported by Nachmani & Wolf (2021). For a fair method-level comparison between diffusion-based decoders, DDECC is trained from scratch using the CrossMPT model as its backbone, instead of the original ECCT backbone.

Main results. Overall, treating decoding as score-based continuous denoising yields consistent improvements over prior methods across code families and rates. Table 1 summarizes the main results. SB-ECC achieves the best BER in

Table 2. Solver trade-offs on selected codes. Entries are $-\ln(\text{BER})$ at $E_b/N_0 \in \{4, 5, 6\}$ dB. N_s is the maximum number of solver steps (see 4.3); inference uses early stopping.

Code	Params	Euler			DPM			Speedup		
		N_s	4	5	6	N_s	4	5	6	%
BCH	(63,36)	9	5.77	8.04	11.17	5	5.77	8.04	11.17	7.40
	(64,32)	7	7.76	10.39	13.72	5	7.76	10.39	13.72	9.95
POLAR	(128,64)	8	8.73	12.63	16.81	6	8.73	12.62	16.82	6.51
	(128,86)	7	7.83	11.05	14.84	5	7.83	11.04	14.85	7.49
LDPC	(49,24)	9	7.69	10.77	14.71	6	7.69	10.77	14.73	8.96
	(121,60)	9	6.33	10.40	16.01	6	6.32	10.38	16.02	12.82

39/42 entries and ties for the best result in one additional entry, with an average SNR gain of ≈ 0.17 dB and a maximum gain of 0.46 dB over the strongest competing baseline. The remaining entries are within a small margin of the best competing method. Figures 2 and 3 provide the corresponding BER and BLER curves for representative code instances. These plots complement the aggregate $-\ln(\text{BER})$ results in Table 1 and show the behavior across the evaluated E_b/N_0 range, including comparisons to stronger BP baselines with 100 and 200 iterations.

5.2. Inference Trade-offs: Solvers and Steps

Solver choice provides a direct latency–accuracy knob at test time, without retraining, we can reduce runtime while preserving error-rate performance. Table 2 compares Euler (Song et al., 2020b) and DPM (Lu et al., 2022) on representative codes, reporting $-\ln(\text{BER})$ at $E_b/N_0 \in \{4, 5, 6\}$ dB and end-to-end decoding time. We discretize uniformly in σ -space and denote by N_s the maximum step budget (§4.3). With early stopping, trajectories often terminate before N_s , practical cost is governed by the realized number

Table 3. Ablation on noise-level conditioning. We report $-\ln(\text{BER})$ (higher is better) at $E_b/N_0 \in \{4, 5, 6\}$ dB for SB-ECC (ours), hard-syndrome conditioning, and predicted-time conditioning.

Method		SB-ECC (ours)			Hard-syndrome			Pred-time cond.		
Code	Params	4	5	6	4	5	6	4	5	6
BCH	(63,36)	5.74	8.12	11.20	5.71	8.04	11.00	5.68	7.90	11.07
POLAR	(64,32)	7.77	10.30	13.78	7.76	10.38	13.63	7.71	10.41	13.61
	(128,64)	9.03	13.13	16.81	8.64	12.47	16.27	8.40	12.26	16.63

of function evaluations. We measure runtime by decoding the same number of samples per SNR using the same checkpoint, batching, and GPU, and report time reduction as $(t_{\text{Euler}} - t_{\text{DPM}})/t_{\text{Euler}} \times 100\%$. Across all tested codes and SNRs, DPM attains essentially the same $-\ln(\text{BER})$ as Euler using a smaller step budget, translating into consistent runtime reductions. Together with early stopping, this yields a simple drop-in path to faster decoding without sacrificing accuracy.

5.3. Ablation Studies

Time Conditioning. We consider the practical setting where the decoder is given only the channel observation \mathbf{y} and has *no access* to the channel SNR (or any other side information) at test time. We therefore study whether providing an auxiliary *noise-level proxy* inferred from \mathbf{y} is beneficial by comparing three training variants of the same backbone.

SB-ECC (ours) is trained exactly as in (12) without providing any time/noise input. Hard-syndrome conditioning, inspired by DDECC, computes the hard-decision syndrome via $\mathbf{y}_b = \text{bin}(\text{sign}(\mathbf{y}))$ and $\mathbf{s}(\mathbf{y}) = H\mathbf{y}_b^\top$. We summarize it by the parity-error count $e(\mathbf{y}) \triangleq \sum_{i=1}^{n-k} s_i(\mathbf{y}) \in \{0, \dots, n-k\}$, embed $e(\mathbf{y})$ with a learned embedding, and inject it by element-wise modulation of the initial token embeddings. Predicted-time conditioning adds a lightweight 2-layer MLP ϕ_θ that predicts the normalized diffusion time $\hat{t} = \phi_\theta(\mathbf{y}, \mathbf{s}(\mathbf{y}))$, and conditions the decoder on \hat{t} . We train it jointly with $\mathcal{L}_{\text{joint}} = (1 - \gamma_{\text{time}})\mathcal{L}_e + \gamma_{\text{time}}\mathcal{L}_t$, where \mathcal{L}_e is (12) and $\mathcal{L}_t = \|\hat{t} - t\|_2^2$, using $\gamma_{\text{time}} = 0.1$. Empirically, SB-ECC performs best (Table 3), suggesting that in our signed-input formulation the decoder can infer the effective noise regime from \mathbf{y} directly. Conditioning on either a syndrome-based proxy or a learned time estimate does not improve performance. This observation is consistent with findings in denoising generative modeling that oracle noise conditioning is not always required and that additional proxy signals can sometimes hurt (Sun et al., 2025), and we find a similar effect in the error-correction setting.

Signed vs. magnitude-only observations. As shown in Table 4, to test whether discarding the sign harms learning

Table 4. Signed vs. magnitude-only input.

Code	Params	Signed \mathbf{y}			Reliability $ \mathbf{y} $		
		4	5	6	4	5	6
BCH	(31,16)	7.33	9.95	13.03	2.93	3.36	3.83
Polar	(64,32)	7.77	10.30	13.78	2.87	3.28	3.77
LDPC	(49,24)	7.74	10.88	14.63	2.84	3.24	3.72

the denoising vector field, we reran training with the *only* modification $\mathbf{y} \leftarrow |\mathbf{y}|$ at the network input, keeping the architecture, optimization, noise schedule, and data generation identical. Across BCH(31, 16), Polar(64, 32), and LDPC(49, 24), the magnitude-only variant fails to learn: the training objective stagnates and decoding performance does not improve over the course of training. For all mentioned codes, the loss quickly plateaus at $\mathcal{L} \approx 5.0 \times 10^{-1}$, consistent with a near-trivial predictor.

Concretely, in the magnitude-only setting the network collapses to a near-zero noise estimator: $\hat{\epsilon}_\theta(\mathbf{y}, \mathbf{s}(\mathbf{y})) \approx \mathbf{0}$, with empirical statistics $\min \approx -0.1$, $\max \approx 0.1$, and $\text{mean} \approx 0$. As a result, the predicted clean estimate satisfies $\hat{\mathbf{x}}_0 \approx \mathbf{y}$, meaning that hard decisions are unchanged:

$$\text{sign}(\hat{\mathbf{x}}_0) = \text{sign}(\mathbf{x}_t) = \text{sign}(\mathbf{y}).$$

Therefore, the overall decoder reduces to uncoded hard-decision detection on the channel output, yielding essentially no coding gain.

6. Conclusion

We presented **SB-ECC**, a score-based decoder that casts soft decoding as continuous-time denoising via the PF-ODE, and learns a *continuous* additive-noise (score) field directly from the *raw signed* channel observation under parity constraints. Across 42 code/SNR settings, SB-ECC achieves the best BER in 39/42 entries, with an average SNR gain of ≈ 0.17 dB and a maximum gain of 0.46 dB over the strongest competing baseline. The formulation also enables a practical latency–accuracy knob at inference: replacing Euler with a higher-order solver (DPM) preserves $-\ln(\text{BER})$ while reducing end-to-end decoding time by 8.86% on average (up to 12.82%). Finally, our results indicate that learning decoding directly from raw observations can generalize to mid-length codes despite codeword-space sparsity, and that recent attention-based architectures make learning such continuous guidance fields feasible in practice.

Impact Statement

This work aims to advance machine learning methods for soft decoding of error-correcting codes. Improved learned decoders may benefit communication and storage systems by increasing robustness and enabling flexible accuracy–latency trade-offs under fixed computational budgets. As with many general-purpose advances in communication technology, the same capabilities could be incorporated into both beneficial and potentially harmful applications depending on the deployment context. We encourage responsible use and consideration of relevant safeguards and regulations when integrating learned decoders into real-world systems.

References

- Arikan, E. Channel polarization: A method for constructing capacity-achieving codes for symmetric binary-input memoryless channels. *IEEE Transactions on Information Theory*, 55(7):3051–3073, 2009.
- Artemasov, D., Andreev, K., Rybin, P., and Frolov, A. Soft-output deep neural network-based decoding. In *2023 IEEE Globecom Workshops (GC Wkshps)*, pp. 1692–1697. IEEE, 2023.
- Austin, J., Johnson, D. D., Ho, J., Tarlow, D., and Van Den Berg, R. Structured denoising diffusion models in discrete state-spaces. *Advances in neural information processing systems*, 34:17981–17993, 2021.
- Bennatan, A., Choukroun, Y., and Kisilev, P. Deep learning for decoding of linear codes—a syndrome-based approach. In *2018 IEEE International Symposium on Information Theory (ISIT)*, pp. 1595–1599. IEEE, 2018.
- Berlekamp, E., McEliece, R., and Van Tilborg, H. On the inherent intractability of certain coding problems (corresp.). *IEEE Transactions on Information Theory*, 24(3): 384–386, 2003.
- Blattmann, A., Dockhorn, T., Kulal, S., Mendelevitch, D., Kilian, M., Lorenz, D., Levi, Y., English, Z., Voleti, V., Letts, A., et al. Stable video diffusion: Scaling latent video diffusion models to large datasets. *arXiv preprint arXiv:2311.15127*, 2023a.
- Blattmann, A., Rombach, R., Ling, H., Dockhorn, T., Kim, S. W., Fidler, S., and Kreis, K. Align your latents: High-resolution video synthesis with latent diffusion models. In *Proceedings of the IEEE/CVF conference on computer vision and pattern recognition*, pp. 22563–22575, 2023b.
- Bose, R. C. and Ray-Chaudhuri, D. K. On a class of error correcting binary group codes. *Information and control*, 3(1):68–79, 1960.
- Buchberger, A., Häger, C., Pfister, H. D., Schmalen, L., and i Amat, A. G. Learned decimation for neural belief propagation decoders. In *ICASSP 2021-2021 IEEE International Conference on Acoustics, Speech and Signal Processing (ICASSP)*, pp. 8273–8277. IEEE, 2021.
- Cammerer, S., Gruber, T., Hoydis, J., and Ten Brink, S. Scaling deep learning-based decoding of polar codes via partitioning. In *GLOBECOM 2017-2017 IEEE global communications conference*, pp. 1–6. IEEE, 2017.
- Chen, N., Zhang, Y., Zen, H., Weiss, R. J., Norouzi, M., and Chan, W. Wavegrad: Estimating gradients for waveform generation. *arXiv preprint arXiv:2009.00713*, 2020.
- Choukroun, Y. and Wolf, L. Denoising diffusion error correction codes. *arXiv preprint arXiv:2209.13533*, 2022a.
- Choukroun, Y. and Wolf, L. Error correction code transformer. *arXiv preprint arXiv:2203.14966*, 2022b.
- Choukroun, Y. and Wolf, L. A foundation model for error correction codes. In *The Twelfth International Conference on Learning Representations*, 2024a.
- Choukroun, Y. and Wolf, L. Learning linear block error correction codes. *arXiv preprint arXiv:2405.04050*, 2024b.
- Cohen, S.-e., Choukroun, Y., and Nachmani, E. Hybrid mamba-transformer decoder for error-correcting codes. *arXiv preprint arXiv:2505.17834*, 2025.
- Dhariwal, P. and Nichol, A. Diffusion models beat gans on image synthesis. *Advances in neural information processing systems*, 34:8780–8794, 2021.
- Gallager, R. Low-density parity-check codes. *IRE Transactions on information theory*, 8(1):21–28, 1962.
- Gruber, T., Cammerer, S., Hoydis, J., and Ten Brink, S. On deep learning-based channel decoding. In *2017 51st annual conference on information sciences and systems (CISS)*, pp. 1–6. IEEE, 2017.
- Hamalainen, A. and Henriksson, J. A recurrent neural decoder for convolutional codes. In *1999 IEEE International Conference on Communications (Cat. No. 99CH36311)*, volume 2, pp. 1305–1309. IEEE, 1999.
- Ho, J., Jain, A., and Abbeel, P. Denoising diffusion probabilistic models. *Advances in neural information processing systems*, 33:6840–6851, 2020.
- Ho, J., Chan, W., Saharia, C., Whang, J., Gao, R., Gritsenko, A., Kingma, D. P., Poole, B., Norouzi, M., Fleet, D. J., et al. Imagen video: High definition video generation with diffusion models. *arXiv preprint arXiv:2210.02303*, 2022a.

- Ho, J., Salimans, T., Gritsenko, A., Chan, W., Norouzi, M., and Fleet, D. J. Video diffusion models. *Advances in neural information processing systems*, 35:8633–8646, 2022b.
- Hyvärinen, A. Estimation of non-normalized statistical models by score matching. *Journal of Machine Learning Research*, 6(24):695–709, 2005.
- Jiang, Y., Kim, H., Asnani, H., and Kannan, S. Mind: Model independent neural decoder. In *2019 IEEE 20th International Workshop on Signal Processing Advances in Wireless Communications (SPAWC)*, pp. 1–5. IEEE, 2019.
- Kamassury, J. K. S. and Silva, D. Iterative error decimation for syndrome-based neural network decoders. *arXiv preprint arXiv:2012.00089*, 2020.
- Karras, T., Aittala, M., Aila, T., and Laine, S. Elucidating the design space of diffusion-based generative models. *Advances in neural information processing systems*, 35:26565–26577, 2022.
- Kingma, D. P. and Ba, J. Adam: A method for stochastic optimization. *arXiv preprint arXiv:1412.6980*, 2014. URL <https://arxiv.org/abs/1412.6980>.
- Kong, Z., Ping, W., Huang, J., Zhao, K., and Catanzaro, B. Diffwave: A versatile diffusion model for audio synthesis. *arXiv preprint arXiv:2009.09761*, 2020.
- Kschischang, F. R., Frey, B. J., and Loeliger, H.-A. Factor graphs and the sum-product algorithm. *IEEE Transactions on information theory*, 47(2):498–519, 2002.
- Lau, C. W. K., Shi, X., Zheng, Z., Cao, H., and Guo, N. Interplay between belief propagation and transformer: Differential-attention message passing transformer. In *2025 IEEE International Symposium on Information Theory (ISIT)*, pp. 1–6. IEEE, 2025.
- LeCun, Y., Bengio, Y., and Hinton, G. Deep learning. *nature*, 521(7553):436–444, 2015.
- Lee, H., Seo, E. Y., Ju, H., and Kim, S.-H. On training neural network decoders of rate compatible polar codes via transfer learning. *Entropy*, 22(5):496, 2020.
- Lei, H., Lau, C. W., Zhou, K., Guo, N., and Farnia, F. Consistency flow model achieves one-step denoising error correction codes. *arXiv preprint arXiv:2512.01389*, 2025.
- Leung, C. T., Bhat, R. V., and Motani, M. Low-latency neural decoders for linear and non-linear block codes. In *2019 IEEE Global Communications Conference (GLOBECOM)*, pp. 1–6. IEEE, 2019a.
- Leung, C. T., Bhat, R. V., and Motani, M. Low-latency neural decoders for linear and non-linear block codes. In *Proc. IEEE Global Communications Conference (GLOBECOM)*, 2019b.
- Levy, M., Choukroun, Y., and Wolf, L. Accelerating error correction code transformers. *arXiv preprint arXiv:2410.05911*, 2024.
- Li, X., Thickstun, J., Gulrajani, I., Liang, P. S., and Hashimoto, T. B. Diffusion-lm improves controllable text generation. *Advances in neural information processing systems*, 35:4328–4343, 2022.
- Lian, M., Carpi, F., Häger, C., and Pfister, H. D. Learned belief-propagation decoding with simple scaling and snr adaptation. In *2019 IEEE International Symposium on Information Theory (ISIT)*, pp. 161–165. IEEE, 2019.
- Liu, L., Ren, Y., Lin, Z., and Zhao, Z. Pseudo numerical methods for diffusion models on manifolds. *arXiv preprint arXiv:2202.09778*, 2022.
- Lu, C., Zhou, Y., Bao, F., Chen, J., Li, C., and Zhu, J. Dpm-solver: A fast ode solver for diffusion probabilistic model sampling in around 10 steps. *Advances in neural information processing systems*, 35:5775–5787, 2022.
- Lugosch, L. and Gross, W. J. Neural offset min-sum decoding. In *2017 IEEE International Symposium on Information Theory (ISIT)*, pp. 1361–1365. IEEE, 2017.
- Lyu, W., Zhang, Z., Jiao, C., Qin, K., and Zhang, H. Performance evaluation of channel decoding with deep neural networks. In *2018 IEEE International Conference on Communications (ICC)*, pp. 1–6. IEEE, 2018.
- Matsumine, T. and Ochiai, H. Recent advances in deep learning for channel coding: A survey. *arXiv preprint arXiv:2406.19664*, 2024.
- Nachmani, E. and Wolf, L. Hyper-graph-network decoders for block codes. *Advances in Neural Information Processing Systems*, 32, 2019.
- Nachmani, E. and Wolf, L. Autoregressive belief propagation for decoding block codes. *arXiv preprint arXiv:2103.11780*, 2021.
- Nachmani, E., Be’ery, Y., and Burshtein, D. Learning to decode linear codes using deep learning. In *2016 54th Annual Allerton Conference on Communication, Control, and Computing (Allerton)*, pp. 341–346. IEEE, 2016.
- Nachmani, E., Marciano, E., Lugosch, L., Gross, W. J., Burshtein, D., and Be’ery, Y. Deep learning methods for improved decoding of linear codes. *IEEE Journal of Selected Topics in Signal Processing*, 12(1):119–131, 2018.

- Nichol, A. Q. and Dhariwal, P. Improved denoising diffusion probabilistic models. In *International conference on machine learning*, pp. 8162–8171. PMLR, 2021.
- O’shea, T. and Hoydis, J. An introduction to deep learning for the physical layer. *IEEE Transactions on Cognitive Communications and Networking*, 3(4):563–575, 2017.
- Park, S.-J., Kwak, H.-Y., Kim, S.-H., Kim, S., Kim, Y., and No, J.-S. How to mask in error correction code transformer: Systematic and double masking. *arXiv preprint arXiv:2308.08128*, 2023.
- Park, S.-J., Kwak, H.-Y., Kim, S.-H., Kim, Y., and No, J.-S. Crossmpt: Cross-attention message-passing transformer for error correcting codes. *arXiv preprint arXiv:2405.01033*, 2024.
- Popov, V., Vovk, I., Gogoryan, V., Sadekova, T., and Kudinov, M. Grad-tts: A diffusion probabilistic model for text-to-speech. In *International conference on machine learning*, pp. 8599–8608. PMLR, 2021.
- Richardson, T. and Urbanke, R. *Modern coding theory*. Cambridge university press, 2008.
- Richardson, T. J. and Urbanke, R. L. The capacity of low-density parity-check codes under message-passing decoding. *IEEE Transactions on information theory*, 47(2): 599–618, 2002.
- Rombach, R., Blattmann, A., Lorenz, D., Esser, P., and Ommer, B. High-resolution image synthesis with latent diffusion models. In *Proceedings of the IEEE/CVF conference on computer vision and pattern recognition*, pp. 10684–10695, 2022.
- Saharia, C., Chan, W., Chang, H., Lee, C., Ho, J., Salimans, T., Fleet, D., and Norouzi, M. Palette: Image-to-image diffusion models. In *ACM SIGGRAPH 2022 conference proceedings*, pp. 1–10, 2022.
- Sattiraju, R., Weinand, A., and Schotten, H. D. Performance analysis of deep learning based on recurrent neural networks for channel coding. In *2018 IEEE International Conference on Advanced Networks and Telecommunications Systems (ANTS)*, pp. 1–6. IEEE, 2018.
- Seo, J., Lee, J., and Kim, K. Decoding of polar code by using deep feed-forward neural networks. In *2018 international conference on computing, networking and communications (ICNC)*, pp. 238–242. IEEE, 2018a.
- Seo, J., Lee, J., and Kim, K. Decoding of polar code by using deep feed-forward neural networks. In *Proc. International Conference on Computing, Networking and Communications (ICNC)*, pp. 238–242, 2018b.
- Sohl-Dickstein, J., Weiss, E., Maheswaranathan, N., and Ganguli, S. Deep unsupervised learning using nonequilibrium thermodynamics. In *International conference on machine learning*, pp. 2256–2265. pmlr, 2015.
- Song, J., Meng, C., and Ermon, S. Denoising diffusion implicit models. *arXiv preprint arXiv:2010.02502*, 2020a.
- Song, Y. and Ermon, S. Generative modeling by estimating gradients of the data distribution. *Advances in neural information processing systems*, 32, 2019.
- Song, Y., Sohl-Dickstein, J., Kingma, D. P., Kumar, A., Ermon, S., and Poole, B. Score-based generative modeling through stochastic differential equations. *arXiv preprint arXiv:2011.13456*, 2020b.
- Sun, Q., Jiang, Z., Zhao, H., and He, K. Is noise conditioning necessary for denoising generative models? *arXiv preprint arXiv:2502.13129*, 2025.
- Vincent, P. A connection between score matching and denoising autoencoders. *Neural computation*, 23(7):1661–1674, 2011.
- Wang, X.-A. and Wicker, S. B. An artificial neural net viterbi decoder. *IEEE Transactions on communications*, 44(2):165–171, 1996.
- Zheng, K., Lu, C., Chen, J., and Zhu, J. Dpm-solver-v3: Improved diffusion ode solver with empirical model statistics. *Advances in Neural Information Processing Systems*, 36:55502–55542, 2023.

Table 5. Iterations to reach zero syndrome (mean \pm std) for Euler decoding with 10 vs. 5 steps, and the corresponding deltas. $\Delta(-\ln \text{BER})$ is computed as (5 steps) – (10 steps), so positive values indicate improved BER.

Code	E_b/N_0	#It (10 steps)	#It (5 steps)	$\Delta\#It$	$\Delta(-\ln \text{BER})$
BCH (63,36)	4	2.92 \pm 1.82	1.68 \pm 0.87	-1.24	-0.09
	5	1.85 \pm 1.31	1.16 \pm 0.71	-0.70	-0.10
	6	1.09 \pm 1.02	0.75 \pm 0.62	-0.34	-0.15
BCH (63,45)	4	1.95 \pm 1.53	1.20 \pm 0.80	-0.75	-0.05
	5	1.12 \pm 1.06	0.76 \pm 0.64	-0.36	-0.10
	6	0.58 \pm 0.78	0.44 \pm 0.54	-0.14	-0.12
BCH (63,51)	4	1.55 \pm 1.51	1.00 \pm 0.81	-0.56	-0.02
	5	0.80 \pm 0.94	0.58 \pm 0.60	-0.22	-0.05
	6	0.38 \pm 0.64	0.30 \pm 0.47	-0.07	-0.08
LDPC (49,24)	4	3.11 \pm 1.53	1.79 \pm 0.81	-1.31	-0.07
	5	2.14 \pm 1.37	1.30 \pm 0.76	-0.84	-0.11
	6	1.34 \pm 1.17	0.88 \pm 0.69	-0.47	-0.05
LDPC (121,60)	4	3.77 \pm 1.23	2.12 \pm 0.62	-1.65	-0.03
	5	2.76 \pm 0.97	1.64 \pm 0.55	-1.13	-0.05
	6	1.94 \pm 0.92	1.21 \pm 0.53	-0.73	-0.05
POLAR (64,48)	4	1.80 \pm 1.32	1.15 \pm 0.77	-0.65	0.01
	5	1.03 \pm 1.04	0.71 \pm 0.64	-0.32	-0.00
	6	0.51 \pm 0.76	0.39 \pm 0.53	-0.12	-0.01
POLAR (128,64)	4	4.20 \pm 1.14	2.35 \pm 0.62	-1.85	-0.10
	5	3.12 \pm 1.07	1.81 \pm 0.59	-1.31	-0.07
	6	2.18 \pm 1.03	1.34 \pm 0.58	-0.84	-0.02
POLAR (128,86)	4	2.70 \pm 1.07	1.61 \pm 0.61	-1.09	-0.06
	5	1.83 \pm 0.95	1.16 \pm 0.54	-0.67	-0.11
	6	1.11 \pm 0.86	0.79 \pm 0.52	-0.32	-0.08
POLAR (128,96)	4	2.32 \pm 1.13	1.42 \pm 0.65	-0.90	-0.03
	5	1.47 \pm 0.93	0.98 \pm 0.53	-0.50	-0.05
	6	0.82 \pm 0.79	0.63 \pm 0.53	-0.20	-0.01

7. Appendix

7.1. Improvement Measured in dB

Figure 4 presents BER curves for representative code instances with large SNR gains of SB-ECC relative to the strongest competing baseline at matched BER. We quantify improvement using *SNR gain*, defined as the reduction in E_b/N_0 required by SB-ECC to achieve the same BER as the best competing baseline. Across the three cases shown in Figure 4, the gains at $E_b/N_0 = 5$ dB are 0.37 dB for BCH(63, 45), 0.37 dB for LDPC(49, 24), and 0.27 dB for BCH(63, 36).

7.2. Early Stopping Behavior and Effective Compute

Table 5 measures how quickly Euler decoding reaches a valid codeword under the parity constraints. At each solver iteration i , we convert the current continuous estimate into bits, $\hat{\mathbf{x}}^{(i)} = \text{bin}(\text{sign}(\mathbf{x}^{(i)}))$, and compute its syndrome. The reported #It is the first iteration index at which the syndrome becomes zero, and the table summarizes this stopping iteration by its mean and standard deviation. This metric is reported alongside BER because the two capture different aspects of decoding. The stopping iteration reflects how fast the solver finds a parity-consistent candidate, while BER

evaluates whether that candidate matches the transmitted codeword. Together, they quantify the effectiveness of early stopping and its impact on accuracy.

Across all code families and SNRs, parity satisfaction occurs in only a few iterations on average. Even when allowing a maximum of 10 solver steps, the mean stopping iteration is typically in the 1-4 range (with decreasing iterations as E_b/N_0 increases), indicating that the PF-ODE trajectory quickly moves into the code manifold. Reducing the solver budget to 5 steps further decreases the stopping iteration (negative $\Delta\#It$), as expected given the smaller iteration horizon.

Importantly, this analysis also clarifies the *latency gap* to one-step decoders. A one-step model corresponds to a single neural evaluation, whereas our method performs multiple evaluations. However, the measured mean iteration counts show that we are not an order of magnitude slower in typical operating regimes: in the mean case we require only a small constant number of updates to reach a valid codeword. This modest increase in compute yields substantial BER improvements over one-step baselines (see main results), highlighting a favorable latency-accuracy trade-off. Several additional denoiser evaluations are sufficient to capture most of the performance gains, while still keeping inference close to one-step latency in practice.

7.3. Scalability to Longer Codes

To further evaluate scalability beyond the block lengths used in the main benchmark, we include additional experiments on longer codes.

Table 6 reports $-\ln(\text{BER})$ at $E_b/N_0 \in \{4, 5, 6\}$ dB for LDPC (204, 102) and LDPC (529, 440). BP is evaluated with 50 decoding iterations. The results suggest that SB-ECC remains competitive on longer codes.

Table 6. Longer LDPC-code results. Values are reported as $-\ln(\text{BER})$ at $E_b/N_0 \in \{4, 5, 6\}$ dB, where higher is better. BP uses 50 decoding iterations.

Code	BP-50			SB-ECC		
	4	5	6	4	5	6
LDPC (204, 102)	10.27	13.79	16.29	11.20	15.78	18.77
LDPC (529, 440)	8.18	14.88	19.74	7.93	15.23	21.70

7.4. Robustness under Rayleigh Fading Channel

The main experiments focus on the standard AWGN setting. Following the Rayleigh-channel evaluation protocol used in ECCT(Choukroun & Wolf, 2022b) and CrossMPT(Park et al., 2024), we additionally evaluate SB-ECC under a Rayleigh fading channel. In this setting, the received signal is

$$\mathbf{y} = \mathbf{h} \odot \mathbf{x}_s + \mathbf{z}, \quad (16)$$

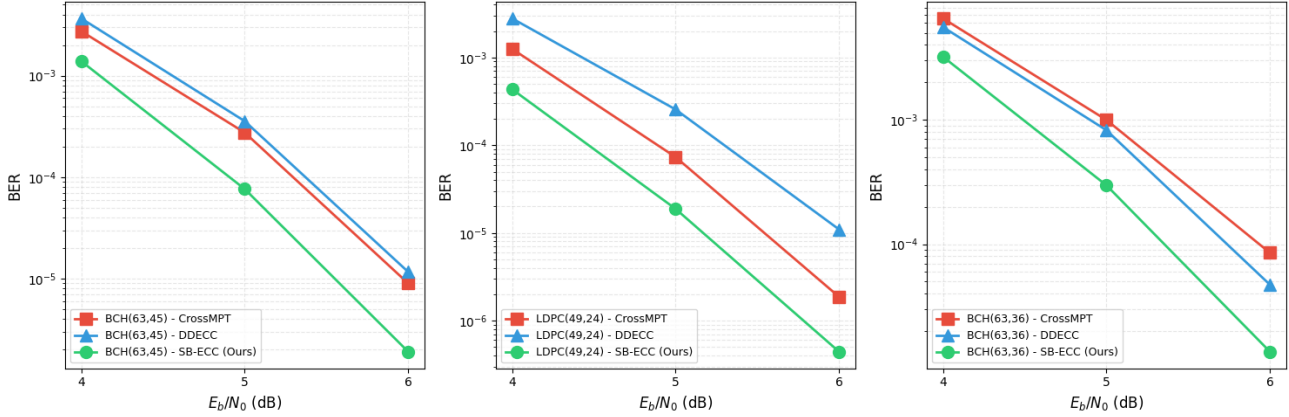


Figure 4. BER versus E_b/N_0 for three representative code instances with large SNR gains of SB-ECC (green). Left to right: BCH(63, 45), LDPC(49, 24), and BCH(63, 36). Markers show simulated operating points at $E_b/N_0 \in \{4, 5, 6\}$ dB (lines connect points). SNR gain is defined as the reduction in E_b/N_0 required by SB-ECC to match the BER of the strongest competing baseline, computed via linear interpolation in the $-\ln(\text{BER})$ domain.

Table 7. Rayleigh-channel inference results using models trained under AWGN. Values are reported as $-\ln(\text{BER})$; higher is better. Best results are marked in bold.

Code	Params	E_b/N_0	BP-50	BP-200	CrossMPT	SB-ECC
LDPC	(121, 70)	4	4.06	4.26	4.25	4.62
		5	5.10	5.48	5.53	6.02
		6	6.34	6.89	7.11	7.92
BCH	(31, 16)	4	3.79	3.99	5.53	5.74
		5	4.36	4.67	6.55	6.86
		6	4.93	5.37	7.61	8.07
CCSDS	(128, 64)	4	5.25	5.59	5.25	5.77
		5	6.78	7.37	6.94	7.70
		6	8.72	9.64	8.92	10.08

where \mathbf{h} is an i.i.d. Rayleigh-distributed fading vector with scale parameter $\alpha = 1$, \odot denotes element-wise multiplication, and $\mathbf{z} \sim \mathcal{N}(\mathbf{0}, \sigma^2 \mathbf{I})$. Importantly, we use the same models trained under AWGN and evaluate them on Rayleigh samples without retraining or fine-tuning.

Table 7 reports $-\ln(\text{BER})$ at $E_b/N_0 \in \{4, 5, 6\}$ dB for BP with 50 and 200 iterations, CrossMPT, and SB-ECC. Across the evaluated code instances, SB-ECC achieves the best result among the available baselines, providing initial evidence that the learned score-based decoder retains useful robustness under a channel shift from AWGN training to Rayleigh inference.

7.5. Comparison with SCL Decoding

We compare SB-ECC with successive cancellation list (SCL) decoding on Polar codes. SCL is a classical Polar-specific decoder and therefore provides a strong specialized reference point for this code family. Table 8 reports $-\ln(\text{BER})$ at $E_b/N_0 \in \{4, 5, 6\}$ dB. The SCL and CrossMPT values are taken from Park et al. (2024), and we add the corresponding SB-ECC results. As expected, the

Polar-specific SCL decoder, especially with list size $L = 4$, remains a very strong baseline and achieves the best result in many settings.

Table 8. Comparison with SCL decoding on Polar codes. Results are reported as $-\ln(\text{BER})$. Higher is better; best results are marked in bold.

Code	E_b/N_0	SCL-1	SCL-4	Cross-MPT	SB-ECC
Polar (64, 32)	4	7.30	8.11	7.50	7.77
	5	9.67	10.70	9.97	10.30
	6	13.18	14.04	13.31	13.78
Polar (64, 48)	4	6.19	6.69	6.51	6.63
	5	8.41	8.63	8.70	8.64
	6	10.97	11.24	11.31	11.27
Polar (128, 64)	4	8.37	9.60	7.52	9.03
	5	11.69	13.16	11.21	13.13
	6	13.70	17.42	14.76	16.94
Polar (128, 86)	4	7.54	9.26	7.86	8.03
	5	10.74	13.04	11.45	11.48
	6	15.14	17.13	15.47	16.10
Polar (128, 96)	4	6.74	8.02	7.15	7.64
	5	9.53	11.60	10.15	10.32
	6	13.53	18.16	13.13	13.37

7.6. Latency and Throughput Compared to External Baselines

We complement the internal solver comparison in Section 5.2 with a direct runtime comparison against external baselines. Since CrossMPT is a one-step decoder, while SB-ECC and DDECC are iterative decoding methods, this comparison should be interpreted as a practical latency-accuracy trade-off rather than as a pure architecture comparison. All measurements are performed under the same hardware setting. For DDECC, we use the public repository implementation without adding an early-stopping rule.

Table 9 reports latency and throughput on BCH (63, 45)

at $E_b/N_0 \in \{3, 4, 5\}$ dB. As expected, the one-step CrossMPT decoder has the lowest latency. SB-ECC requires multiple denoising evaluations, but is substantially faster than the evaluated DDECC implementation across all tested SNRs. We note, however, that this runtime gap is partly implementation-dependent; adding a parity-check-based early-stopping criterion to DDECC would likely reduce its latency and increase its throughput, and may therefore move its practical runtime closer to SB-ECC.

Table 9. Latency and throughput comparison on BCH (63, 45). Latency is reported in milliseconds and throughput in samples/sec.

Method	Latency (ms)			Throughput		
	3 dB	4 dB	5 dB	3 dB	4 dB	5 dB
SB-ECC	49.96	30.76	18.34	20.02	32.51	54.53
CrossMPT	14.69	14.55	14.48	68.08	68.71	69.04
DDECC	266.06	266.85	265.10	3.76	3.75	3.77